chemosensors

Article

Au-Decorated Polyaniline-ZnO Electrospun Composite Nanofiber Gas Sensors with Enhanced Response to NO_2 Gas

Maryam Bonyani [1], Seyed Mojtaba Zebarjad [1,*], Kamal Janghorban [1], Jin-Young Kim [2], Hyoun Woo Kim [3,4] and Sang Sub Kim [2,*]

[1] Department of Materials Science and Engineering, Shiraz University, Shiraz 71557-13876, Iran
[2] Department of Materials Science and Engineering, Inha University, Incheon 22212, Korea
[3] Division of Materials Science and Engineering, Hanyang University, Seoul 04763, Korea
[4] The Research Institute of Industrial Science, Hanyang University, Seoul 04763, Korea
* Correspondence: mojtabazebarjad@shirazu.ac.ir (S.M.Z.); sangsub@inha.ac.kr (S.S.K.)

Abstract: Ternary systems are less studied for sensing applications due to complex synthesis procedures. However, they have more sources of resistance modulation, leading to an enhanced gas response. In this study, a ternary system, namely Au-decorated ZnO-polyaniline (PANI) composite nanofibers with different amounts of PANI (10, 25, and 50 wt.%) were synthesized for NO_2 gas sensing studies. First, ZnO nanofibers were synthesized by electrospinning, and then an Au layer (9 nm) was coated on the ZnO nanofibers. Finally, PANI was coated onto the prepared Au-decorated ZnO nanofibers. NO_2 gas sensing investigations indicated that the sensor with 25 wt.% PANI had the best response to NO_2 gas at 300 °C. In addition, the optimized sensor exhibited high selectivity to NO_2 gas. The improved performance of the optimal gas sensor was attributed to the role of Au, the formation of ZnO-PANI heterojunctions, and the optimal amount of PANI. The promising effect of this ternary system for NO_2 sensing was demonstrated, and it can be extended to other similar systems.

Keywords: NO_2 gas; ZnO; PANI; Au decoration; nanofiber; gas sensor

check for updates

Citation: Bonyani, M.; Zebarjad, S.M.; Janghorban, K.; Kim, J.-Y.; Kim, H.W.; Kim, S.S. Au-Decorated Polyaniline-ZnO Electrospun Composite Nanofiber Gas Sensors with Enhanced Response to NO_2 Gas. *Chemosensors* **2022**, *10*, 388. https://doi.org/10.3390/chemosensors10100388

Academic Editor: James Covington

Received: 5 August 2022
Accepted: 21 September 2022
Published: 24 September 2022

Publisher's Note: MDPI stays neutral with regard to jurisdictional claims in published maps and institutional affiliations.

Copyright: © 2022 by the authors. Licensee MDPI, Basel, Switzerland. This article is an open access article distributed under the terms and conditions of the Creative Commons Attribution (CC BY) license (https://creativecommons.org/licenses/by/4.0/).

1. Introduction

Modern life has resulted in increasing amounts of pollutant gases in the environment [1]. Nitrogen dioxide (NO_2) gas, with dangerous and oxidizing effects, is emitted mainly from fossil fuel combustion and chemical factories [2]. Exposure to NO_2 can result in respiratory diseases, including bronchitis, pulmonary edema, pharyngeal, and asthma [3], and aggravate existing heart conditions [4]. In addition, it can cause acid rain and photochemical smog [5,6]. Further, even at low concentrations, it has negative effects on the human immune system and nervous system and can inhibit cell growth [7,8]. Therefore, developing reliable gas sensors for monitoring NO_2 gas is essential [9].

Even though gas chromatography and liquid chromatography techniques can be used for the detection of gases, they are time-consuming, bulky, expensive, slow in response, have high power requirements, and need expert operators [3]. Therefore, gas sensors with small size, online response, and low prices are preferred to the above techniques [10].

Metal oxide semiconductors are widely used for the realization of resistive gas sensors [8,11–14]. Variations in the resistance in the presence of target gas are the basic mechanism of gas sensing in this type of gas sensor [15,16]. Among them, ZnO is an n-type (Eg = 3.37 eV) semiconductor and is extensively used in resistive-based gas sensors because of its high stability and high mobility of charge carriers [17–19]. WO_3 is a well-known material for NO_2 gas sensing [20]. However, ZnO, with the above-mentioned merits, is also another promising material for sensing NO_2 gas, and many papers have reported NO_2 gas sensing properties of ZnO [21–23].

Pure ZnO generally suffers from poor selectivity and a high sensing temperature [24]. Accordingly, various strategies such as the addition of dopants [25], noble metal functionalization [26], hybrid material fabrication [27], morphology engineering [28], and heterojunction formation [29] are used to enhance the sensing capacity of ZnO-based gas sensors. Among these, hybrid formation with conducting polymers (CPs) is highly popular because of the synergistic effects of ZnO and CPs [30]. In CPs, a conjugated carbon chain comprised of alternating double and single bonds exists, in which the highly delocalized, polarized, and electron-dense π bonds contribute to conduction [31]. Therefore, they can be used for gas and bio-sensing studies [32,33]. Among different CPs, polyaniline (PANI) has advantages such as low cost, low-temperature synthesis, good flexibility, and high stability [34]. PANI structure consists of benzene structural units and quinoid structural units [35]. Previously, PANI was used for NO_2 gas sensing studies. It was used in the pristine form [36,37] and in combination with other materials such as ZnO [38–40] or other materials [41,42]. Therefore, hybrids of ZnO-PANI are highly desirable for sensing applications [43]. In particular, ZnO nanofibers exhibit a high surface area for the gas molecules. Thus, composite nanofibers of ZnO and PANI are good candidates for sensing applications.

The use of noble metals is advantageous for further improving the sensitivity of composite nanofibers [44]. Generally, noble metals such as Au, with a work function different from that of metal oxides, can form Schottky junctions, and modulation of potential barriers in these junctions can induce resistance changes, attributing to the sensing mechanism [45]. Furthermore, Au exhibits good catalytic activity toward gases [46–49]. Au as decoration on other materials has been used for NO_2 gas sensing [50–54]. Therefore, in this work, we chose it for decoration on the surface of the sensing materials.

The novelty of this work is the combination of Au, PANI, and ZnO in the form of an electrospun composite nanofiber for NO_2 gas sensing. As far as we know, there is no study related to gas sensing features of the ternary system of Au-ZnO-PANI in the literature. Therefore, we designed a new ternary composite nanofiber for NO_2 gas sensing studies. Different amounts of PANI (10, 25, and 50 wt.%) were added to Au-decorated ZnO nanofibers to study the effect of PANI on the NO_2 gas response of the resultant ternary composite. The results indicated that the sensor with 25 wt.% PANI exhibited the best response to NO_2 gas at 300 °C. In addition, the optimized gas sensor exhibited high selectivity for NO_2 gas. The improved performance of the optimal sensor was attributed to the promising role of Au, the formation of ZnO-PANI heterojunctions, and the optimal amount of PANI.

2. Materials and Methods

2.1. Materials

Analytical grade PANI (99.5%), zinc acetate [$Zn((CH_3CO_2)_2)$], ammonium persulfate (APS) (98%), polyvinyl alcohol (PVA, MW ~80,000), D-camphor-10-sulfonic acid (CSA) [$(C_{10}H_{16}O_4S)$], and chloroform (90%) were obtained from Merck and used as the starting materials.

2.2. Preparation of ZnO Nanofibers

Initially, 10 wt.% PVA was dissolved in distilled water at 65–70 °C. Then, zinc acetate (7 wt.%) was added to the resultant solution and stirred for 2 h at 70 °C to obtain a viscous solution for the electrospinning process (Spinner 3X-Advance, Shiraz, Iran). After loading the solution into a stainless steel needle-attached glass syringe, a positive voltage of 16 kV was applied to the needle. Consequently, the nanofibers were generated and collected on a collector placed at a fixed distance of 14 cm. The feeding rate was set to 0.5 mL/h, and the ambient temperature was 25 °C. In order to remove the organic materials, the composites were annealed (600 °C/2 h). The resultant crystalline nanofibers were used for further processing.

2.3. Au Decoration

A layer of Au (9 nm) was coated onto the synthesized ZnO nanofibers via sputtering (Quorum Technologies, Lewes, UK). The input power was 30 W, the deposition temperature was 25 °C, there was a 100 mm distance between the Au target, the substrate was 10 cm, and the deposition pressure was 10 mTorr. Then, the samples were annealed at 450 °C for 0.5 h in a muffle furnace to form isolated Au NPs.

2.4. Preparation of Composite Nanofibers

First, in situ polymerization of PANI was performed in an ice/water bath (0−5 °C for 5 h). Different amounts of PANI in 20 mL of chloroform were mixed with 0.05 M CSA by continuous stirring at 0–5 °C. Subsequently, 20 mL of a chloroform solution containing APS was slowly added to initiate polymerization. The molar ratio of aniline to APS was 1:1. The temperature for the polymerization reaction was fixed at 0–5 °C for 5 h. Upon polymerization, the resulting residue was sonicated and poured onto the ZnO nanofibers. Finally, the ZnO-PANI composite nanofibers were washed with water and dried at 55 °C for one day.

2.5. Characterization

The morphology of the synthesized nanofibers was examined using scanning electron microscopy (SEM; TESCAN-Vega 3, Brno, Czech Republic) and transmission electron microscopy (TEM; Philips, CM 200). X-ray diffraction (XRD; Bruker D8-ADVANCE) studies were performed to explore the phases and crystallinities of the products. In order to study the thermal behavior of the products, thermogravimetric analysis (TGA; TA Q600, New Castle, Delaware, USA) was carried out at 25–700 °C. Fourier transform infrared (FTIR, Bruker, Bremen, Germany) spectra were obtained to ascertain the different bonds in the products.

2.6. Gas Sensing Measurements

SiO_2-grown Si (100) substrates (1 × 1 cm^2) equipped with Ti (50 nm)/Pt (200 nm) bilayer interdigitated electrodes were used as sensor substrates. The gap size between electrodes was 250 μm. In order to prepare the gas sensors, a slurry was prepared from the synthesized materials in α-terpineol (10 μL). Subsequently, it was drop-coated onto a substrate and dried. The thickness of the sensing layer was approximately 30 μm. Finally, it was annealed in air at 300 °C for 2 h. Gas sensing evaluations were performed in a chamber inside a horizontal tubular quartz furnace with the possibility of temperature control. Appropriate gas concentrations were injected into the gas chamber using mass flow controllers. NO_2 gas was dry air background. Thus, NO_2 gas measurement was performed under dry conditions. The total gas flow rate was 500 sccm. The resistance was measured using a homemade data acquisition system (LabView, National Instruments) via a Keithley 2400 source meter. The resistance of the sensor was constantly recorded in the air (R_a) and gas atmospheres (R_g), and the response was evaluated using $R = R_g/R_a$ for NO_2 gas and $R = R_a/R_g$ for the interfering gases.

3. Results and Discussion

3.1. Morphological, Structural, and Thermal Studies

Figure 1a shows the SEM image of the Au-decorated ZnO nanofibers. Au NPs are decorated on ZnO nanofibers as isolated NPs. This shows a good combination for gas sensing studies. Moreover, Figure 1b–d show the SEM images of the ZnO-PANI composite nanofibers with 10, 25, and 50 wt.% PANI, respectively. In all cases, the diameter of the ZnO nanofibers increased because of the presence of PANI. In addition, for the sample with 50 wt.% PANI, many ZnO nanofibers are bonded together, which ultimately decreases the overall surface area of the ZnO nanofibers. This can have a negative effect on sensing studies.

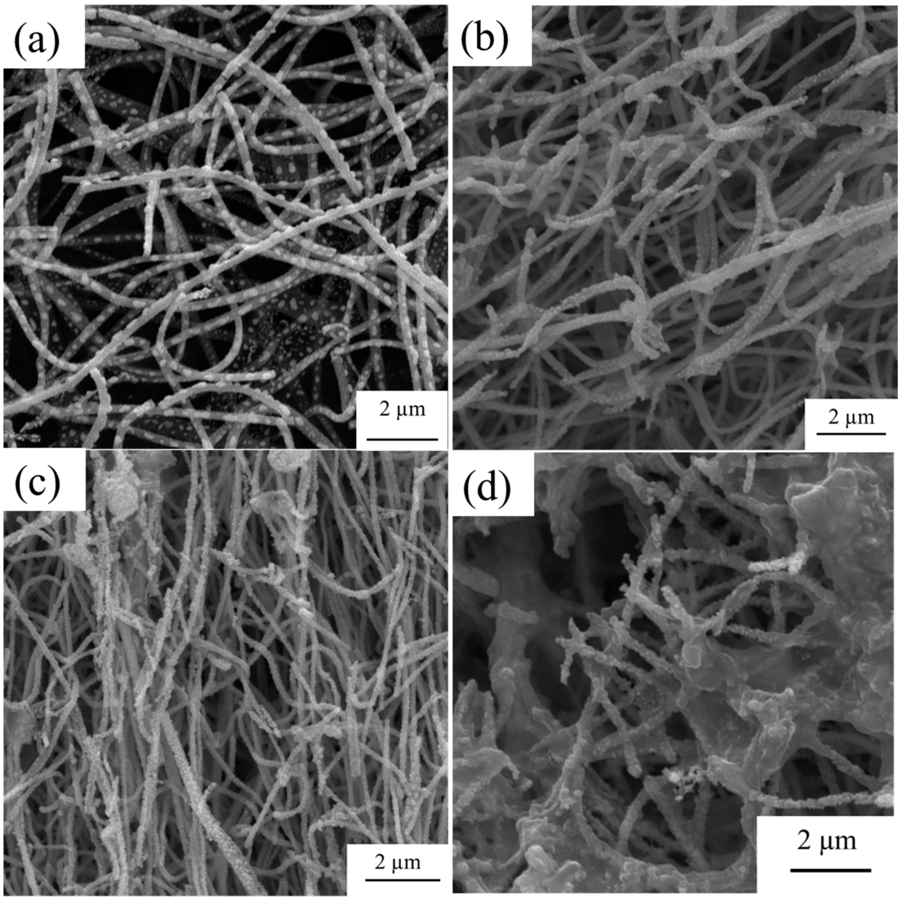

Figure 1. SEM micrographs of (**a**) Au-decorated ZnO nanofibers and Au-decorated ZnO-PANI composite nanofibers with different amounts of PANI; (**b**) 10; (**c**) 25; (**d**) 50 wt.%.

Further studies were performed using TEM analysis. Figure 2a–c reveals the TEM images of Au-decorated ZnO-PANI (25 wt.%) composite nanofibers at different magnifications; the diameter of the nanofiber was approximately 400 nm. Figure 2a clearly shows the formation of a long nanofiber, and in Figure 2b,c, the presence of Au nanoparticles on the surface of ZnO nanofiber is quite observable. The size of Au NPs is in the range of ~10 to 30 nm. Figure 2d exhibits the high-resolution TEM (HRTEM) image of Au-decorated ZnO-PANI (25 wt.%) composite nanofibers. Based on TEM images in Figure 2, the shortest spacings between the fringes are 0.280 and 0.240 nm, matching the (100) crystalline plane of ZnO and the (111) crystalline plane of Au, respectively.

Figure 3a indicates the EDS analysis of the Au-decorated ZnO-PANI (25 wt.%) composite nanofibers. Peaks related to the presence of ZnO, PANI, and Au, namely Zn, O, Au, N, and C, are observed. The inset table inside Figure 3a shows the atomic and weight percent of different elements. Figure 3b shows the EDS mapping, in which the distribution of C, N, O, Zn, and Au in the synthesized composite nanofibers is shown. Moreover, Figure 3c,d shows EDS elemental point analysis and mapping analysis results of Au-decorated ZnO-PANI (25 wt.%) composite nanofibers after gas sensing measurements. As shown, there are no noticeable differences in chemical composition before and after gas sensing measurements.

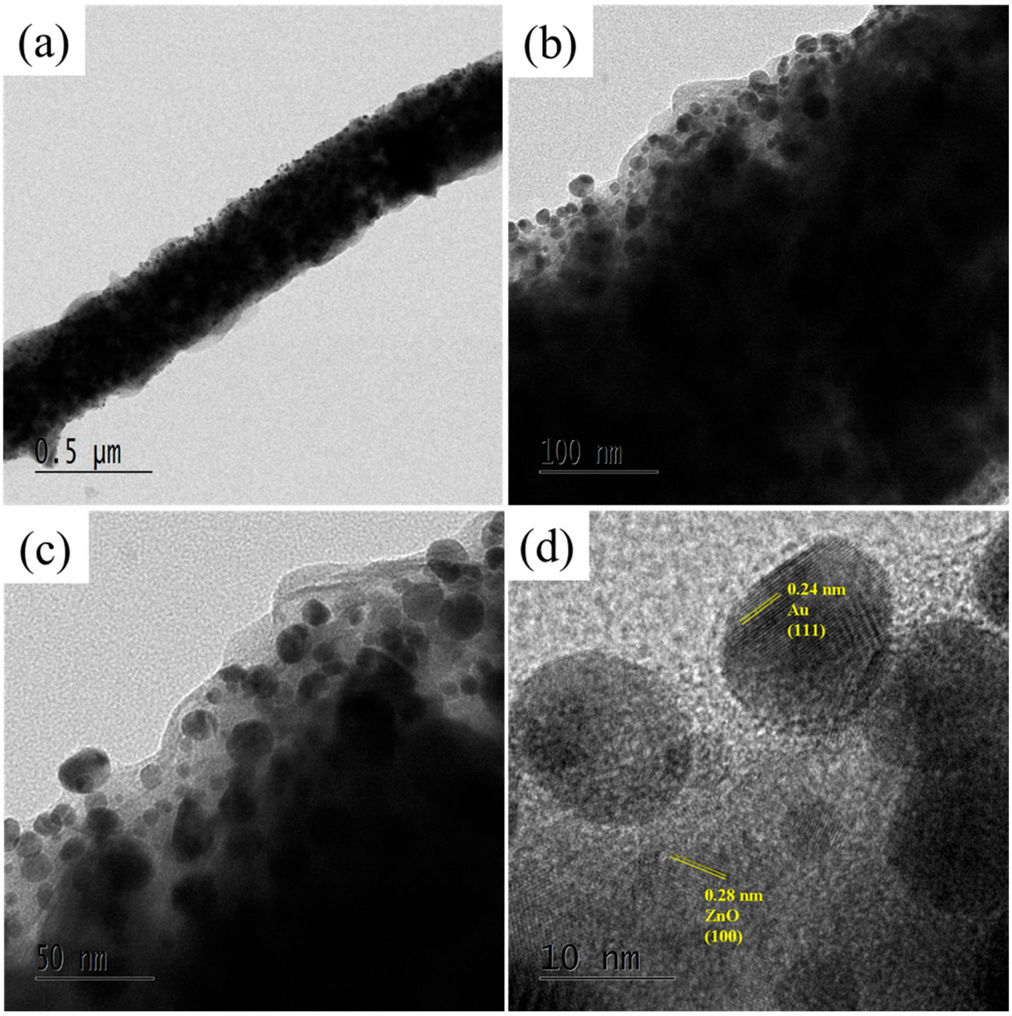

Figure 2. (**a**–**c**) TEM micrographs of Au-decorated ZnO-PANI (25 wt.%) composite nanofibers at three different magnifications; (**d**) corresponding HRTEM image.

Figure 4 offers the XRD patterns of Au-decorated ZnO-PANI composite nanofibers with different amounts of PANI (10, 25, and 50 wt.%), along with standard patterns of ZnO and Au. In all cases, peaks related to ZnO, Au, and PANI are observed without any other crystalline phases. The peaks related to ZnO correspond to hexagonal ZnO (JCPDS Card No. 89–1397) [55]. In addition, the peaks related to Au at 38.15° and 44.4° attributed to the (111) and (200) planes, respectively, are matched with JCPDS Card No. 04–0784, corresponding to the face-centered cubic structure of Au [56]. The weak peaks related to PANI in the XRD patterns reveal partial crystallinity due to the repetition of the benzenoid and quinoid rings in the PANI chains [49].

Figure 5 presents the FTIR spectra of Au-decorated ZnO nanofibers and Au-decorated ZnO-PANI composite nanofibers with different amounts of PANI (10, 25, and 50 wt.%). For Au-decorated ZnO, the strong peak at ~471 cm^{-1} was due to the vibration of Zn–O [38]. For the composite nanofibers, the band at 3450 cm^{-1} is attributed to N–H stretching [57]. The peaks at 1567 and 1481 cm^{-1} were due to the stretching vibrations of the quinone and benzene rings, respectively [58]. The 1297 cm^{-1} band was matched with the C–N stretching vibration [59]. The in-plane and out-of-plane bending of the C–H stretching of PANI are observed at 1115 and 800 cm^{-1}, respectively [60].

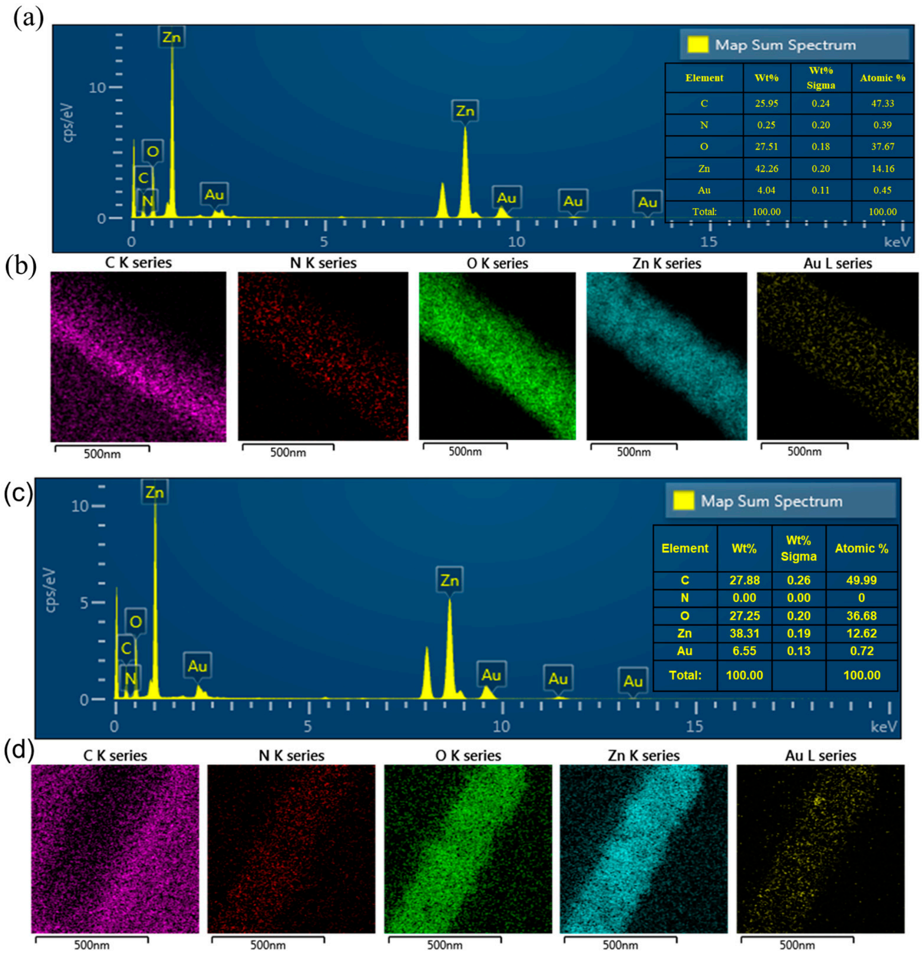

Figure 3. (**a**) EDS analysis (table in inset shows chemical analysis) and (**b**) EDS elemental mapping of Au-decorated ZnO-PANI (25 wt.%) composite nanofibers before gas sensing tests; (**c**) EDS analysis (table in inset shows chemical analysis); (**d**) EDS elemental mapping of Au-decorated ZnO-PANI (25 wt.%) composite nanofibers after gas sensing tests.

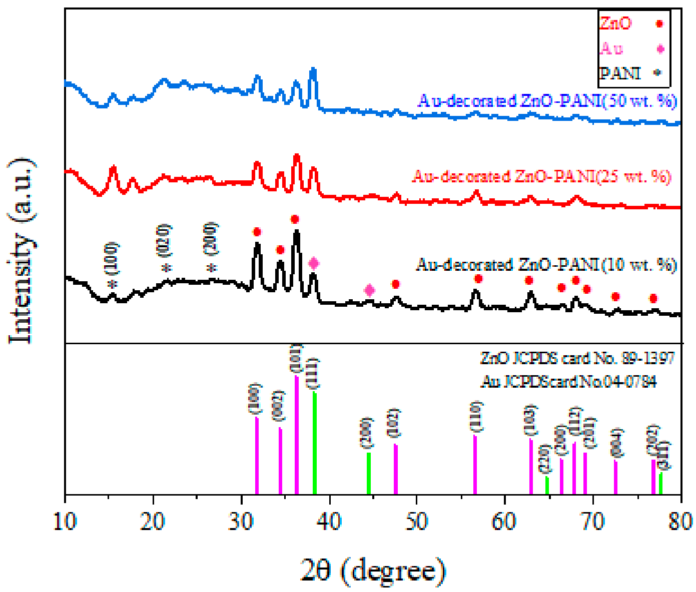

Figure 4. XRD patterns of Au-decorated ZnO-PANI composite nanofibers with different amounts of PANI (10, 25, and 50 wt.%).

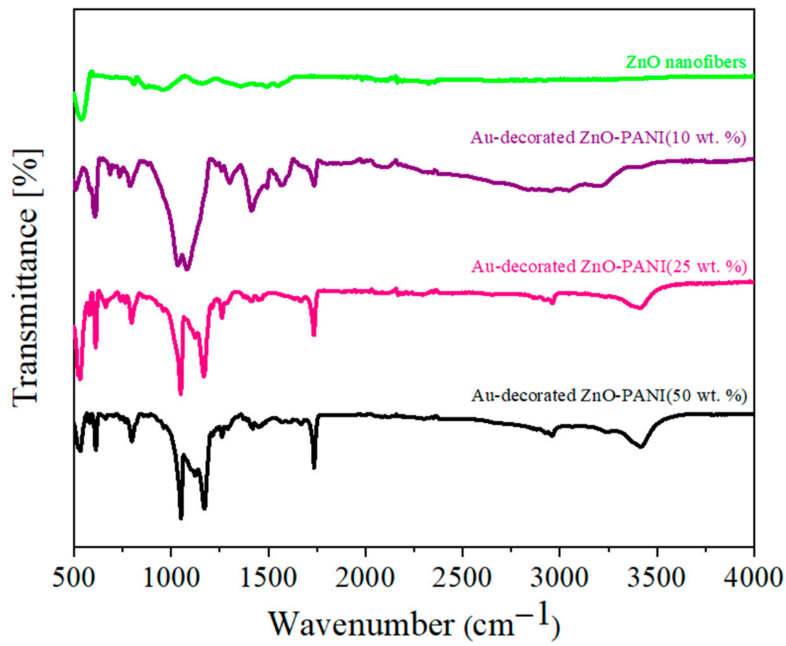

Figure 5. FTIR spectra of Au-decorated ZnO nanofibers and Au-decorated ZnO-PANI composite nanofibers with different amounts of PANI (10, 25, and 50 wt.%).

Figure 6 shows the TGA curve of Au-decorated ZnO-PANI (25 wt.%) composite nanofibers under slow heating from room temperature to 700 °C. Based on the TGA curve, the weight loss of the sample gradually increases with temperature up to approximately 550 °C. The weight loss observed from 25 °C to 100 °C is related to the loss of absorbed water [61]. In the temperature range of 100 to approximately 550 °C, the weight loss is due to the degradation and decomposition of organic materials and the backbone units of PANI [62,63].

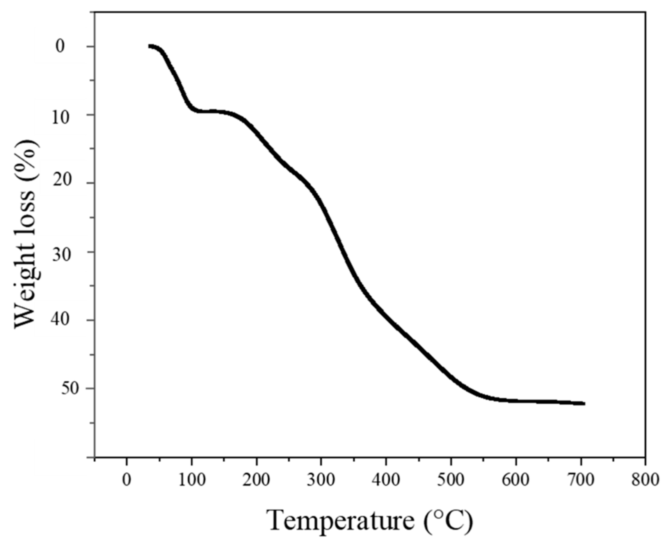

Figure 6. TGA curve of Au-decorated ZnO-PANI (25 wt.%) composite nanofibers.

3.2. Gas Sensing Investigations

Figure 7 offers the dynamic resistance plots of Au-decorated ZnO-PANI composite nanofibers with different amounts of PANI (10, 25, and 50 wt.%) to 10, 30, and 50 ppm NO_2 gas at 300 °C. All sensors exhibited a significant response to NO_2 gas. In addition, the resistance of all gas sensors increased in the NO_2 gas environment, reflecting the n-type feature of gas sensors stemming from the n-type character of ZnO [64].

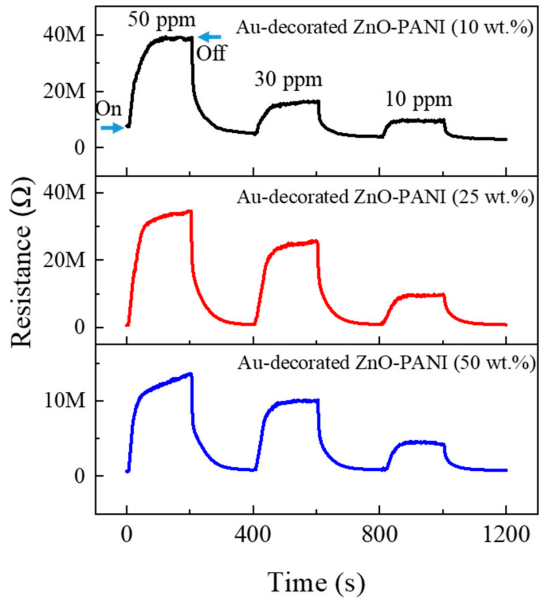

Figure 7. Dynamic resistance graphs of the Au-decorated ZnO-PANI (10, 25, and 50 wt.%) composite nanofiber sensors to 10, 30, and 50 ppm NO_2 gas at 300 °C.

For a better comparison, we depicted the calibration curves of different gas sensors in Figure 8a,c for the sensors with 10, 25, and 50 wt.% PANI, respectively. In all cases, the responses increased with increasing NO_2 gas concentration. In addition, the response showed an almost linear dependence on the NO_2 gas concentration. Figure 8d summarizes the responses of all sensors with different amounts of PANI at various concentrations of NO_2 gas. The sensor with 25 wt.% PANI indicated the highest response to NO_2 gas; therefore, it was selected for further gas sensing studies. Moreover, the sensor with 50 wt.% PANI showed a higher response relative to the sensor with the lowest amount of PANI (10 wt. %).

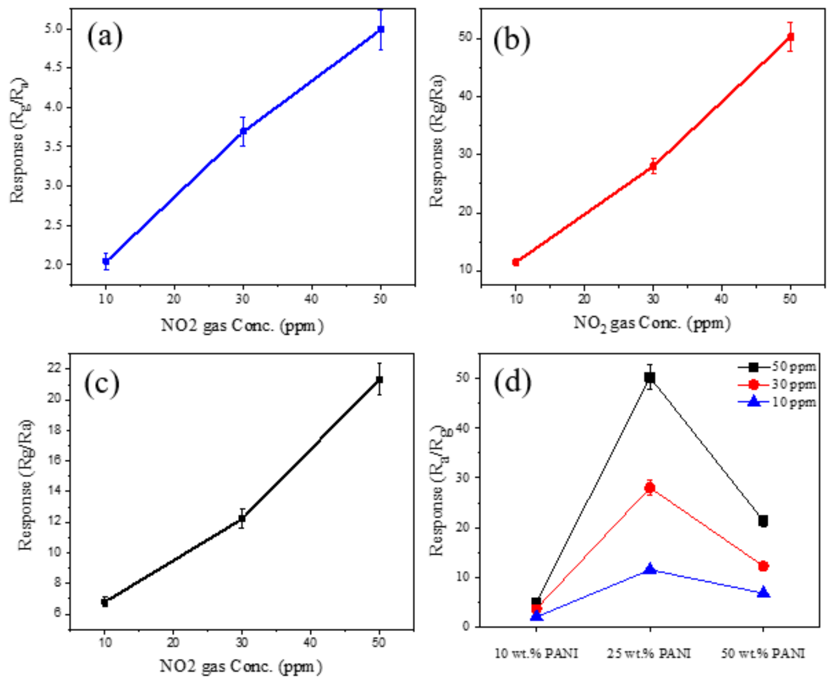

Figure 8. Calibration curves of (**a**) Au-decorated ZnO-PANI (10 wt.%); (**b**) Au-decorated ZnO-PANI (25 wt.%); (**c**) Au-decorated ZnO-PANI (50 wt.%) composite nanofiber gas sensors to NO_2 gas at 300 °C; (**d**) Response of composite nanofiber gas sensors to 10, 30, and 50 ppm NO_2 gas.

Next, we exposed the optimized gas sensor to various amounts of NO_2 gas at various temperatures (Figure 9a). We first tested higher concentrations, and then they gradually decreased. It should be noted that when the sensing temperature is increased, the base resistance is decreased, as shown in Figure 9b. This shows the semiconducting behavior of the gas sensor [65] and is due to the jumping of electrons from the valence band of ZnO to the conduction band, increasing the conductivity. Moreover, possible structural changes of the composite at high temperatures may contribute to the increase in conductivity.

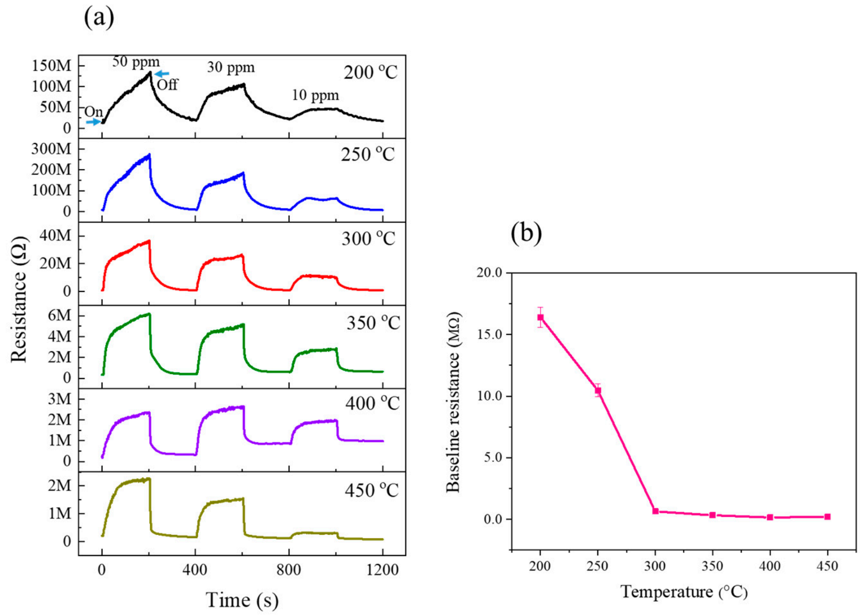

Figure 9. (**a**) Dynamic resistance curves of Au-decorated ZnO-PANI (25 wt.%) composite nanofiber gas sensor to 10, 30, and 50 ppm NO_2 gas (200–450 °C); (**b**) Baseline resistance vs. temperature.

Figure 10 exhibits the response of the optimized gas sensor versus temperature. Such bell shape graph is also reported for other gas sensors [66,67]. Initially, the response slowly increases with temperature, and the response peak is observed at 300 °C; the response then decreases. In particular, at lower temperatures, gas molecules cannot overcome the barrier for adsorption; therefore, the amount of adsorbed gas is low. However, at very high temperatures, the desorption rate is high, resulting in a decrease in the response [68]. It should be noted that the base resistance of the optimal gas sensor at 300 °C was approximately 700 kΩ.

From a practical point of view, a gas sensor should be selective to a particular gas; otherwise, false alarms result, or the sensor cannot show the presence of a toxic gas [69]. Figure 11a gives the selectivity graphs of the optimized gas sensor for some gases at 300 °C. Except for NO_2, the others (CO, H_2, and NH_3) are reducing gases, and the resistance of the gas sensor decreased in the presence of these gases. Figure 11b shows the selectivity pattern of the optimized gas sensor. The responses to 50 ppm H_2, CO, NH_3, and NO_2 gases were 1.6, 1.4, 1.4, and 50, respectively. Thus, the sensor exhibited excellent selectivity for NO_2, which is highly important for practical applications.

For optimal gas sensors, we made three sensors to see reproducibility behavior, as shown in Figure 12. Negligible variations demonstrate good reproducibility of the gas sensor.

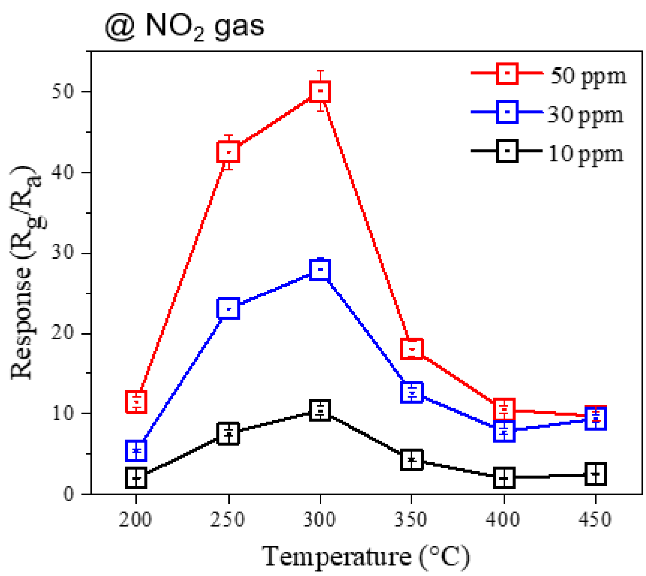

Figure 10. Response vs. sensing temperature of Au-decorated ZnO-PANI (25 wt.%) composite nanofiber gas sensor.

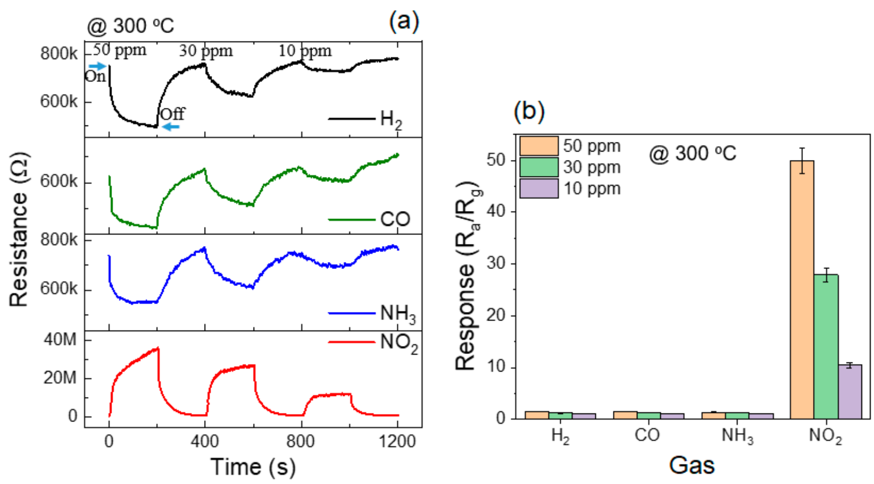

Figure 11. (**a**) Dynamic resistance graphs of Au-decorated ZnO-PANI (25 wt.%) composite nanofiber gas sensor to 10, 30, and 50 ppm of various gases at 300 °C; (**b**) Selectivity graph of Au-decorated ZnO-PANI (25 wt.%) composite nanofiber gas sensor to interfering gases at 300 °C.

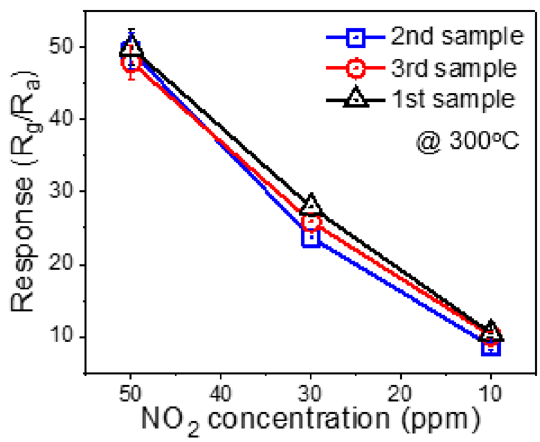

Figure 12. Reproducibility of optimized gas sensor.

Figure 13a shows the repeatability of the optimized gas sensor to 10 ppm NO_2 gas at 300 °C during six sequential cycles, and the corresponding response versus cycle number is shown in Figure 13b. Overall, the response shows negligible variations, demonstrating good repeatability.

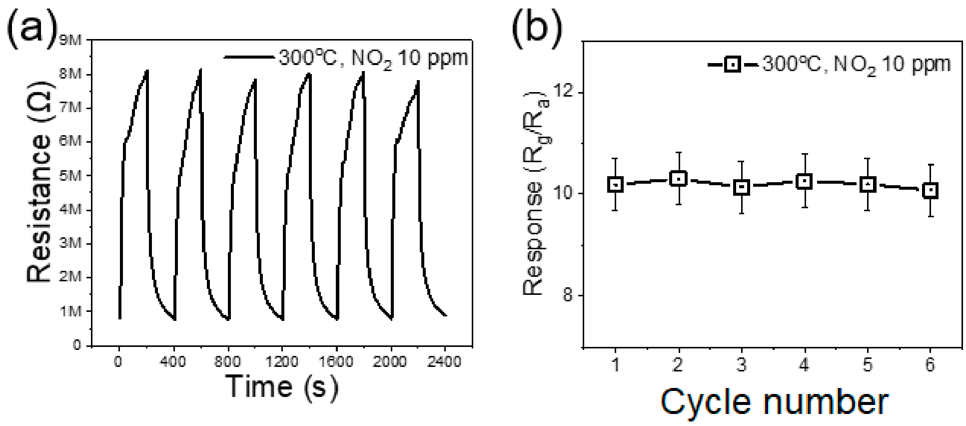

Figure 13. Repeatability of optimized gas sensor (**a**) exposure to six sequential NO_2 (10 ppm) cycles. (**b**) Corresponding response versus cycle number.

Finally, we checked the long-term stability of the optimized gas sensor after one month. Figure 14a,b exhibits dynamic resistance curves and corresponding calibration curves of fresh and after one more keeping in the laboratory to various concentrations of NO_2 gas at 300 °C. Overall, the sensor shows good stability to NO_2 gas even after one month. It should be mentioned that, in general, the stability of resistive-based gas sensors is good [70], and they can be reused many times (3 years or more) [71].

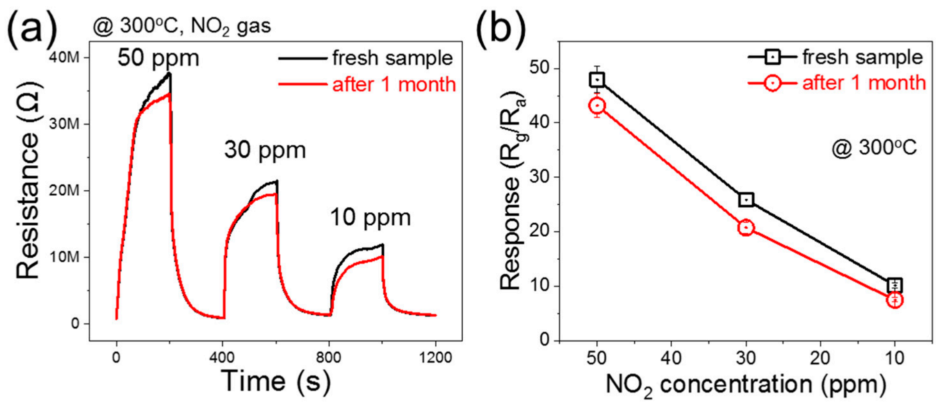

Figure 14. Long-term stability study of optimized gas sensor to various concentrations of NO_2 gas at 300 °C after one month. (**a**) dynamic resistance curves; (**b**) corresponding calibration curves.

3.3. Gas Sensing Mechanism

The modulation of resistance is the basic mechanism of resistive sensors [72]. Initially, in air, oxygen molecules are adsorbed on the surface of the sensing layer, and because of the high electron affinity, electrons are adsorbed from the sensing layer. The relevant reactions are represented as follows [73]:

$$O_2(g) \rightarrow O_2(ads) \quad (1)$$

$$O_2(ads) + e^- \rightarrow O_2^- \quad (2)$$

$$O_2^- + e^- \rightarrow 2O^- \quad (3)$$

$$O^- + e^- \rightarrow O^{2-} \quad (4)$$

The dominant oxygen species differ depending on the sensing temperature [74]. Due to electron abstraction, an electron depletion layer (EDL) is formed on the surface of the gas sensor. Consequently, the resistance increases relative to the vacuum condition. NO_2 gas has an unpaired electron and a strong electron-withdrawing feature [75]. Therefore, the following reactions can occur [76–78]:

$$NO_2(g) \rightarrow NO_2(ads) \quad (5)$$

$$NO_2(ads) + e^- \rightarrow NO_2^- \quad (6)$$

$$NO_2^-(ads) + e^- + O_2^- \rightarrow NO(g) + 2O^- + NO_2^-(ads) \quad (7)$$

$$NO_2^-(ads) + 2e^- + O^- \rightarrow 2O^{2-} + NO(g) \quad (8)$$

Accordingly, more electrons are acquired from the sensor surface, leading to a greater widening of the EDL and an increase in the sensor resistance.

For ZnO-PANI composite nanofibers, because of the difference in the work functions of PANI and ZnO, p-n heterojunctions are formed at the interfaces between ZnO and PANI [79,80]. PANI is normally of p-type semiconductor (E_g = 2.8 eV) because, during the polymerization process, aniline is used, which acts as a dopant for PANI molecules [38]. Electrons from n-type ZnO flow towards PANI with p-type semiconductor behavior until the Fermi levels become equal in the contact areas. Thereby, band bending occurs, and potential barriers are formed at the interfaces (Figure 15a). In the NO_2 atmosphere, due to the abstraction of more electrons by NO_2 gas, the width of the heterojunctions increases, resulting in an increase in the resistance (Figure 15b) [81]. A similar mechanism was reported elsewhere [41]. Indeed, PANI has many electron-rich amino groups, which favor the adsorption of NO_2 gas on the surface of PANI, and as an oxidizing gas, NO_2 converts PANI emeraldine salt to its higher oxidation state [82,83].

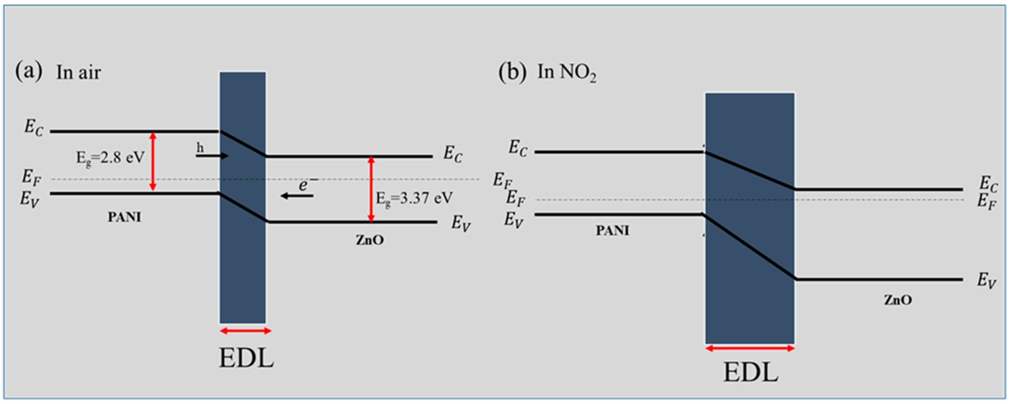

Figure 15. Formation of ZnO-PANI heterojunctions in (**a**) air and (**b**) in the presence of NO_2 gas.

Furthermore, the role of Au NPs should be considered. As shown in Figure 16a,b, due to the high work function of Au NPs (5.1 eV) in the contact areas between Au and ZnO (~4.1 eV), Schottky barriers are formed, resulting in the formation of potential barriers between ZnO and Au [84]. In the presence of NO_2 gas, the height of the barriers increases, resulting in an increase in sensor resistance (Figure 16b). Furthermore, Au NPs exhibit catalytic activity, and incoming oxygen molecules are adsorbed on Au NPs, become dissociated, and via the subsequent spill-over mechanism, are adsorbed on ZnO, thereby leading to the adsorption of more oxygen species [85].

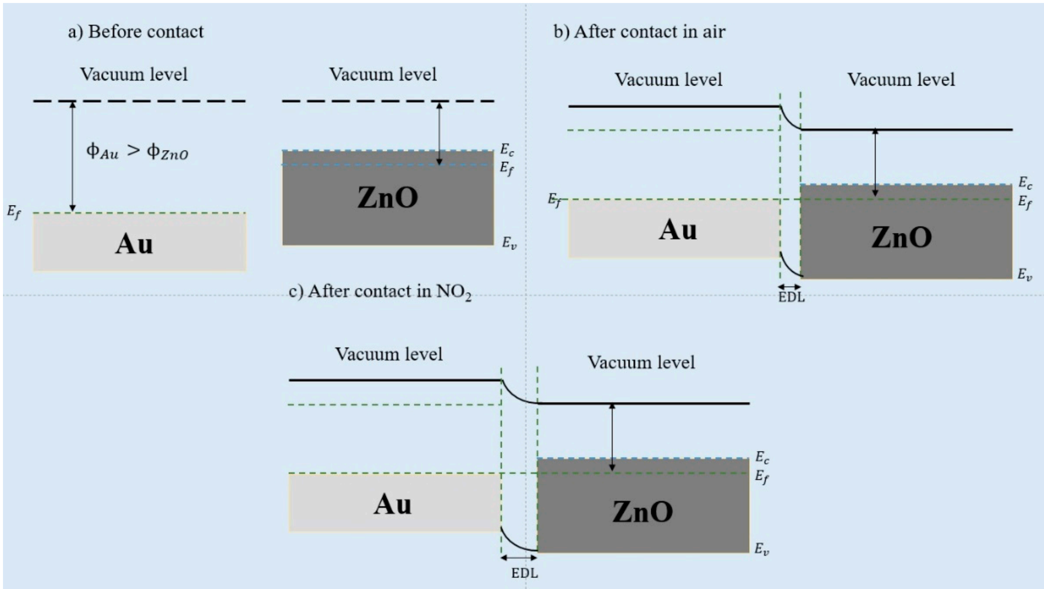

Figure 16. (**a**) Energy level of Au and ZnO before contact. Formation of Schottky barriers between Au and ZnO in (**b**) air and (**c**) NO_2 gas.

In this study, the sensor containing 25 wt.% PANI indicated the highest response to NO_2 gas. When the amount of PANI is lower (10 wt.%), the number of heterojunctions between ZnO and PANI is insufficient to modulate the sensor resistance. In addition, when the PANI content is higher than the optimal value (50 wt.%), due to the intrinsic higher response of ZnO to NO_2 gas and lesser available surface area of ZnO, the response again decreases. At the optimal amount of PANI (25 wt.%), the optimal amount of ZnO-PANI heterojunctions and the large available sensing area of ZnO lead to the best response to NO_2 gas [86].

The selectivity of the optimized gas sensor to NO_2 can be attributed to the high electron affinity (2.28 eV) of NO_2 and the ease of electron capture by this gas. Moreover, the nitrogen atom has one unpaired electron, which facilitates the adsorption of NO_2 on the sensor surface [87,88]. Furthermore, the sensing temperature can be regarded as another factor that affects the selectivity of NO_2 gas.

4. Conclusions

NO_2 sensors based on Au-decorated ZnO-PANI composite nanofibers with different amounts of PANI (10, 25, and 50 wt.%) were fabricated. The morphology, crystal structure, and chemical composition of Au-decorated ZnO-PANI composite nanofibers were analyzed using SEM, TEM, and XRD characterization techniques. The sensor with 25 wt.% PANI exhibited the highest response to NO_2 gas at 300 °C and, in addition, showed excellent selectivity to NO_2 gas. The improved performance of the optimal gas sensor was related to the presence of Au, formation of n-ZnO-p-PANI heterojunctions, and the optimal amount of PANI. Even though we did not examine the response of optimal gas sensors in the presence of humidity, like many other resistive-based gas sensors, the response decreases in the presence of humidity. Moreover, sensing temperature is relatively high, which results in an increase in power consumption. A good solution can be the operation of a gas sensor in self-heating mode to decrease power consumption. Finally, the performance of the gas sensor could be improved by optimizing the amount of Au.

Author Contributions: Conceptualization, S.M.Z. and K.J.; methodology, M.B.; formal analysis, M.B.; investigation, M.B. and J.-Y.K., writing—original draft preparation, M.B., H.W.K. and S.S.K.; writing—review and editing, S.M.Z. and K.J. supervision, S.M.Z. and K.J. All authors have read and agreed to the published version of the manuscript.

Funding: This study was supported by the Korea Polar Research Institute (KOPRI) grant funded by the Ministry of Oceans and Fisheries (KOPRI project No. PE22900) and a National Research Foundation of Korea (NRF) grant funded by the Korean government (MSIT) [No. 2021R1A2C1009790].

Institutional Review Board Statement: Not applicable.

Informed Consent Statement: Not applicable.

Data Availability Statement: Data will be made available on request.

Acknowledgments: The authors are grateful to Shiraz University.

Conflicts of Interest: The authors declare no conflict of interest.

References

1. Sharma, N.; Kumar, S.; Gupta, A.; Dolmanan, S.B.; Patil, D.S.K.; Tan, S.T.; Tripathy, S.; Kumar, M. MoS_2 Functionalized AlGaN/GaN Transistor based Room Temperature NO_2 Gas Sensor. *Sens. Actuator A Phys.* **2022**, *342*, 113647. [CrossRef]
2. Rani, S.; Kumar, M.; Sheoran, H.; Singh, R.; Singh, V.N. Rapidly Responding Room Temperature NO_2 gas Sensor based on SnSe Nanostructured Film. *Mater. Today Commun.* **2022**, *30*, 103135. [CrossRef]
3. Li, Q.; Zeng, W.; Li, Y. Metal oxide gas sensors for detecting NO_2 in industrial exhaust gas: Recent developments. *Sens. Actuators B Chem.* **2022**, *359*, 131579. [CrossRef]
4. Hong, H.S.; Ha, N.H.; Thinh, D.D.; Nam, N.H.; Huong, N.T.; Hue, N.T.; Hoang, T.V. Enhanced sensitivity of self-powered NO_2 gas sensor to sub-ppb level using triboelectric effect based on surface-modified PDMS and 3D-graphene/CNT network. *Nano Energy* **2021**, *87*, 106165. [CrossRef]
5. Kumar, R.R.; Murugesan, T.; Dash, A.; Hsu, C.-H.; Gupta, S.; Manikandan, A.; Kumar Anbalagan, A.; Lee, C.-H.; Tai, N.-H.; Chueh, Y.-L. Ultrasensitive and light-activated NO_2 gas sensor based on networked MoS_2/ZnO nanohybrid with adsorption/desorption kinetics study. *Appl. Surf. Sci.* **2021**, *536*, 147933. [CrossRef]
6. Zhang, C.; Hong, X.; Jiang, C.; Luo, F.; Wan, B. Zheng, X. A special gas sensor based on mesoporous WO_3 sensing electrode in medium low temperature for NO_2 detection. *Mater. Lett.* **2022**, *306*, 130927. [CrossRef]
7. Sun, J.; Xiong, W.; Zhang, J.; Zhang, Y.; Xie, B. SnS_2 nanoparticle-based gas sensor with highly sensitive NO_2 detection at room temperature. *Mater. Lett.* **2022**, *308*, 131214. [CrossRef]
8. Su, P.-G.; Yu, J.-H. Enhanced NO_2 gas-sensing properties of Au-Ag bimetal decorated MWCNTs/WO_3 composite sensor under UV-LED irradiation. *Sens. Actuator A Phys.* **2020**, *303*, 111718. [CrossRef]
9. Bharathi, P.; Harish, S.; Mathankumar, G.; Mohan, M.K.; Archana, J.; Kamalakannan, S.; Prakash, M.; Shimomura, M.; Navaneethan, M. Solution processed edge activated Ni-MoS_2 nanosheets for highly sensitive room temperature NO2 gas sensor applications. *Appl. Surf. Sci.* **2022**, *600*, 154086. [CrossRef]
10. Andrysiewicz, W.; Krzekinski, J.; Skarzynski, K.; Marszalek, K.; Sloma, M.; Rydosz, A. Flexible gas sensor printed on a polymer substrate for sub-ppm acetone detection. *Electron. Mater. Lett.* **2020**, *16*, 146–155. [CrossRef]
11. Kim, S.; Bang, J.H.; Choi, M.S.; Oum, W.; Mirzaei, A.; Lee, N.; Kwon, H.C.; Lee, D.; Jeon, H.; Kim, S.S.; et al. Synthesis, characterization and gas-sensing properties of pristine and SnS_2 functionalized TeO_2, nanowires. *Met. Mater. Int.* **2019**, *25*, 805–813. [CrossRef]
12. Park, S.; Kheel, H.; Sun, G.J.; Kim, H.W.; Ko, T.; Lee, C. Room-temperature hydrogen gas sensing properties of the networked Cr_2O_3-functionalized Nb_2O_5 nanostructured sensor. *Met. Mater. Int.* **2016**, *22*, 730–736. [CrossRef]
13. Kim, S.S.; Na, H.G.; Kwon, Y.J.; Cho, H.Y.; Kim, H.W. Synthesis and room-temperature NO_2 sensing properties of Sb_2O_5 nanowires. *Met. Mater. Int.* **2015**, *21*, 415–421. [CrossRef]
14. Kim, J.H.; Zheng, Y.; Mirzaei, A.; Kim, H.W.; Kim, S.S. Synthesis and selective sensing properties of rGO/metal-coloaded SnO_2 nanofibers. *J. Elec. Mater.* **2017**, *46*, 3531–3541. [CrossRef]
15. Li, T.; Yin, W.; Gao, S.; Sun, Y.; Xu, P.; Wu, S.; Kong, H.; Yang, G.; Wei, G. The combination of two-dimensional nanomaterials with metal oxide nanoparticles for gas sensors: A review. *Nanomaterials.* **2022**, *12*, 982. [CrossRef]
16. Güntner, A.T.; Pineau, N.J.; Pratsinis, S.E. Flame-made chemoresistive gas sensors and devices. *Prog. Energy Combust. Sci.* **2022**, *90*, 100992. [CrossRef]
17. Franco, M.A.; Conti, P.P.; Andre, R.S.; Correa, D.S. A review on chemiresistive ZnO gas sensors. *Sens. Actuators Rep.* **2022**, *4*, 100100. [CrossRef]
18. Chen, Y.; Li, H.; Huang, D.; Wang, X.; Wang, Y.; Wang, W.; Yi, M.; Cheng, Q.; Song, Y.; Han, G. Highly sensitive and selective acetone gas sensors based on modified ZnO nanomaterials. *Mater. Sci. Semi. Proc.* **2022**, *148*, 106807. [CrossRef]
19. Syue, Y.-K.; Hsu, K.-C.; Fang, T.-H.; Lee, C.-I.; Shih, C.-J. Characteristics and gas sensor applications of ZnO-Perovskite heterostructure. *Ceram. Int.* **2022**, *48*, 12585–12591. [CrossRef]
20. Zhang, Z.; Wen, Z.; Ye, Z.; Zhu, L. Ultrasensitive ppb-level NO_2 gas sensor based on WO_3 hollow nanosphers doped with Fe. *Appl. Surf. Sci.* **2018**, *434*, 891–897. [CrossRef]
21. Kumar, R.; Al-Dossary, O.; Kumar, G.; Umar, A. Zinc oxide nanostructures for NO_2 gas–sensor applications: A review. *Micro Nano Lett.* **2015**, *7*, 97–120. [CrossRef]

22. Khudiar, S.S.; Nayef, U.M.; Mutlak, F.A.H.; Abdulridha, S.K. Characterization of NO_2 gas sensing for ZnO nanostructure grown hydrothermally on porous silicon. *Optik* **2022**, *249*, 168300. [CrossRef]
23. Wang, J.; Yang, Y.; Xia, Y. Mesoporous MXene/ZnO nanorod hybrids of high surface area for UV-activated NO_2 gas sensing in ppb-level. *Sens. Actuators B Chem.* **2022**, *353*, 131087. [CrossRef]
24. Lontio Fomekong, R.; Saruhan, B. Influence of humidity on NO_2-sensing and selectivity of spray-CVD grown ZnO thin film above 400 °C. *Chemosensors* **2019**, *7*, 42. [CrossRef]
25. Chang, C.-J.; Lin, C.-Y.; Chen, J.-K.; Hsu, M.-H. Ce-doped ZnO nanorods based low operation temperature NO_2 gas sensors. *Ceram. Int.* **2014**, *40*, 10867–10875. [CrossRef]
26. Wang, J.; Fan, S.; Xia, Y.; Yang, C.; Komarneni, S. Room-temperature gas sensors based on ZnO nanorod/Au hybrids: Visible-light-modulated dual selectivity to NO_2 and NH_3. *J. Haz. Mater.* **2020**, *381*, 120919. [CrossRef]
27. Sonker, R.K.; Yadav, B.; Gupta, V.; Tomar, M. Fabrication and characterization of ZnO-TiO_2-PANI (ZTP) micro/nanoballs for the detection of flammable and toxic gases. *J. Haz. Mater.* **2019**, *370*, 126–137. [CrossRef]
28. Liu, J.; Zhang, L.; Fan, J.; Zhu, B.; Yu, J. Triethylamine gas sensor based on Pt-functionalized hierarchical ZnO microspheres. *Sens. Actuators B Chem.* **2021**, *331*, 129425. [CrossRef]
29. Sun, L.; Sun, J.K.; Zhang, X.; Sun, S.; Bai, Y.; Zhao, R.; Luo, D.; Li Chen, A. rGO functionalized α-Fe_2O_3/Co_3O_4 heterojunction for NO_2 detection. *Sens. Actuators B Chem.* **2022**, *354*, 131194. [CrossRef]
30. Zhu, L.; Zeng, W. Room-temperature gas sensing of ZnO-based gas sensor: A review. *Sens. Actuator A Phys.* **2017**, *267*, 242–261. [CrossRef]
31. Namsheer, K.; Rout, C.S. Conducting polymers: A comprehensive review on recent advances in synthesis, properties and applications. *RSC Adv.* **2021**, *11*, 5659–5697.
32. Wong, Y.C.; Ang, B.C.; Haseeb, A.S.M.A.; Baharuddin, A.A.; Wong, Y.H. Conducting polymers as chemiresistive gas sensing materials: A review. *J. Electrochem. Soc.* **2019**, *167*, 037503. [CrossRef]
33. Ramanavicius, S.; Ramanavicius, A. Conducting polymers in the design of biosensors and biofuel cells. *Polymers.* **2020**, *13*, 49. [CrossRef]
34. Kumar, V.; Mirzaei, A.; Bonyani, M.; Kim, K.-H.; Kim, H.W.; Kim, S.S. Advances in electrospun nanofiber fabrication for polyaniline (PANI)-based chemoresistive sensors for gaseous ammonia. *Trends Analyt. Chem.* **2020**, *129*, 115938. [CrossRef]
35. Li, Z.; Gong, L. Research progress on applications of polyaniline (PANI) for electrochemical energy storage and conversion. *Materials* **2020**, *13*, 548. [CrossRef]
36. Tiwari, A.; Kumar, R.; Prabaharan, M.; Pandey, R.R.; Kumari, P.; Chaturvedi, A.; Mishra, A.K. Nanofibrous polyaniline thin film prepared by plasma-induced polymerization technique for detection of NO2 gas. *Polym. Adv. Technol.* **2010**, *21*, 615–620. [CrossRef]
37. Sonker, R.K.; Yadav, B.C.; Dzhardimalieva, G.I. Preparation and properties of nanostructured PANI thin film and its application as low temperature NO2 sensor. *J. Inorg. Organomet. Polym. Mater.* **2016**, *26*, 1428–1433. [CrossRef]
38. Xu, H.; Chen, X.; Zhang, J.; Wang, J.; Cao, B.; Cui, D. NO_2 gas sensing with SnO_2–ZnO/PANI composite thick film fabricated from porous nanosolid. *Sens. Actuators B Chem.* **2013**, *176*, 166–173. [CrossRef]
39. Sonker, R.K.; Yadav, B.C.; Sharma, A.; Tomar, M.; Gupta, V. Experimental investigations on NO_2 sensing of pure ZnO and PANI–ZnO composite thin films. *RSC Adv.* **2016**, *6*, 56149–56158. [CrossRef]
40. Jain, S.; Karmakar, N.; Shah, A.; Shimpi, N.G. Development of Ni doped ZnO/polyaniline nanocomposites as high response room temperature NO2 sensor. *Mater. Sci. Eng. B* **2019**, *247*, 114381. [CrossRef]
41. Sonker, R.K.; Yadav, B.C. Development of Fe_2O_3–PANI nanocomposite thin film based sensor for NO_2 detection. *J. Taiwan Inst. Chem. Eng.* **2017**, *77*, 276–281. [CrossRef]
42. He, W.; Zhao, Y.; Xiong, Y. Bilayer polyaniline–WO3 thin-film sensors sensitive to NO_2. *ACS Omega* **2020**, *5*, 9744–9751. [CrossRef]
43. Guan, Y.; Wang, C.; Yu, H.; Zou, Z.; Zhou, Y.; Cao, G.; Yao, J. Flexible ZnO/PANI/nonwoven nanocomposite based high-sensitive NH_3 gas sensor via vapor phase polymerization method. *Mater. Sci. Energy Technol.* **2020**, *3*, 862–867. [CrossRef]
44. Lupan, O.; Ababii, N.; Santos-Carballal, D.; Terasa, M.I.; Magariu, N.; Zappa, D.; Comini, E.; Pauporte, T.; Siebert, L.; Faupel, F.; et al. Tailoring the selectivity of ultralow-power heterojunction gas sensors by noble metal nanoparticle functionalization. *Nano Energy* **2021**, *88*, 106241. [CrossRef]
45. Korotcenkov, G.; Brinzari, V.; Cho, B.K. Conductometric gas sensors based on metal oxides modified with gold nanoparticles: A review. *Microchim. Acta* **2016**, *183*, 1033–1054. [CrossRef]
46. Zhao, C.; Shen, J.; Xu, S.; Wei, J.; Liu, H.; Xie, S.; Pan, Y.; Zhao, Y.; Zhu, Y. Ultra-efficient trimethylamine gas sensor based on au nanoparticles sensitized WO_3 nanosheets for rapid assessment of seafood freshness. *Food Chem.* **2022**, *392*, 133318. [CrossRef]
47. Lee, H.Y.; Bang, J.H.; Majhi, S.M.; Mirzaei, A.; Shin, K.Y.; Yu, D.J.; Oum, W.; Kang, S.; Lee, M.L.; Kim, S.S. Conductometric ppb-level acetone gas sensor based on one-pot synthesized Au@ Co_3O_4 core-shell nanoparticles. *Sens. Actuators B Chem.* **2022**, *359*, 131550. [CrossRef]
48. Guo, L.; Shen, Z.; Ma, C.; Ma, C.; Wang, J.; Yuan, T. Gas sensor based on MOFs-derived Au-loaded SnO_2 nanosheets for enhanced acetone detection. *J. Alloys Compd.* **2022**, *906*, 164375. [CrossRef]
49. Hsueh, T.-J.; Wu, S.-S. Highly sensitive Co_3O_4 nanoparticles/MEMS NO_2 gas sensor with the adsorption of the Au nanoparticles. *Sens. Actuators B Chem.* **2021**, *329*, 129201. [CrossRef]

50. Fan, Y.Y.; Tu, H.L.; Pang, Y.; Wei, F.; Zhao, H.B.; Yang, Y.; Ren, T.L. Au-decorated porous structure graphene with enhanced sensing performance for low-concentration NO_2 detection. *Rare Metals* **2020**, *39*, 651–658. [CrossRef]
51. Ponnuvelu, D.V.; Dhakshinamoorthy, J.; Prasad, A.K.; Dhara, S.; Kamruddin, M.; Pullithadathil, B. Geometrically controlled Au-decorated ZnO heterojunction nanostructures for NO_2 detection. *ACS Appl. Nano Mater.* **2020**, *3*, 5898–5909. [CrossRef]
52. Liang, J.; Zhu, K.; Yang, R.; Hu, M. Room temperature NO_2 sensing properties of Au-decorated vanadium oxide nanowires sensor. *Ceram. Int.* **2018**, *44*, 2261–2268. [CrossRef]
53. Cai, Z.; Kim, K.K.; Park, S. Room temperature detection of NO_2 gas under UV irradiation based on Au nanoparticle-decorated porous ZnO nanowires. *J. Mater. Res. Technol.* **2020**, *9*, 16289–16302. [CrossRef]
54. Rattan, S.; Kumar, S.; Goswamy, J.K. Gold nanoparticle decorated graphene for efficient sensing of NO_2 gas. *Sens. Int.* **2022**, *3*, 100147. [CrossRef]
55. Muñoz-Fernandez, L.; Gomez-Villalba, L.S.; Milošević, O.; Rabanal, M.E. Influence of nanoscale defects on the improvement of photocatalytic activity of Ag/ZnO. *Mater. Charact.* **2022**, *185*, 111718. [CrossRef]
56. Farooq, N.; ur Rehman, A.; Qureshi, A.M.; ur Rehman, Z.; Ahmad, A.; Aslam, M.K.; Javed, H.M.A.; Hussain, S.; Habila, M.A.; AlMasoud, N.; et al. Au@ GO@ g-C_3N_4 and Fe_2O_3 nanocomposite for efficient photocatalytic and electrochemical applications. *Surf. Interfaces* **2021**, *26*, 101399. [CrossRef]
57. Lin, C.K.; Kuo, J.L. Anharmonic IR spectra of solvated ammonium and aminium ions: Resemblance between water and bisulfate solvations. *Phys. Chem. Chem. Phys.* **2022**, *24*, 20318–20325. [CrossRef]
58. Zhu, C.; Xue, H.; Zhao, H.; Fei, T.; Liu, S.; Chen, Q.; Gao, B.; Zhang, T. A dual-functional polyaniline film-based flexible electrochemical sensor for the detection of pH and lactate in sweat of the human body. *Talanta* **2022**, *242*, 123289. [CrossRef]
59. Yang, W.; Sun, J.; Liu, D.; Fu, W.; Dong, Y.; Fu, Y.; Zhu, Y. Rational design of hierarchical structure of carbon@ polyaniline composite with enhanced microwave absorption properties. *Carbon* **2022**, *194*, 114–126. [CrossRef]
60. Kumar, A.; Kumar, A.; Mudila, H.; Kumar., V. Synthesis and thermal analysis of polyaniline (PANI). In *Journal of Physics: Conference Series*; IOP Publishing: Bristol, UK, 2020.
61. Henaish, A.M.A.; Salem, B.I.; Meaz, T.M.; Alibwaini, Y.A.; Ajlouni, A.W.; Hemeda, O.M.; Arrasheed, E.A. Synthesize, characterization, dielectric, linear and nonlinear optical properties of Ni–Al Ferrite/PANI nanocomposite film. *Opt. Mater.* **2021**, *119*, 111397. [CrossRef]
62. Pandimurugan, R.; Thambidurai, S. Synthesis of seaweed-ZnO-PANI hybrid composite for adsorption of methylene blue dye. *J. Environ. Chem. Eng.* **2016**, *4*, 1332–1347. [CrossRef]
63. Khairy, M.; Gouda, M.E. Electrical and optical properties of nickel ferrite/polyaniline nanocomposite. *J. Adv. Res.* **2015**, *6*, 555–562. [CrossRef] [PubMed]
64. Shaikh, S.K.; Ganbavale, V.V.; Mohite, S.V.; Patil, U.M.; Rajpure, K.Y. ZnO nanorod based highly selective visible blind ultra-violet photodetector and highly sensitive NO_2 gas sensor. *Superlattices Microstruct.* **2018**, *120*, 170–186. [CrossRef]
65. Gao, H.; Yu, Q.; Chen, K.; Sun, P.; Liu, F.; Yan, X.; Liu, F.; Lu, G. Ultrasensitive gas sensor based on hollow tungsten trioxide-nickel oxide (WO_3-NiO) nanoflowers for fast and selective xylene detection. *J. Colloid Interface Sci.* **2019**, *535*, 458–468. [CrossRef] [PubMed]
66. Tonezzer, M.; Hieu, N.V. Size-dependent response of single-nanowire gas sensors. *Sens. Actuators B Chem.* **2012**, *163*, 146–152. [CrossRef]
67. Arifin, P.; Mustajab, M.A.; Haryono, S.; Adhika, D.R.; Nugraha, A.A. MOCVD growth and characterization of TiO_2 thin films for hydrogen gas sensor application. *Mater. Res. Express* **2019**, *6*, 076313. [CrossRef]
68. Bao, C.; Chen, M.; Jin, X.; Hu, D.; Huang, Q. Efficient and stable photocatalytic reduction of aqueous hexavalent chromium ions by polyaniline surface-hybridized ZnO nanosheets. *J. Mol. Liq.* **2019**, *279*, 133–145. [CrossRef]
69. Korotcenkov, G.; Cho, B.K. Engineering approaches for the improvement of conductometric gas sensor parameters: Part 1. Improvement of sensor sensitivity and selectivity (short survey). *Sens. Actuators B Chem.* **2013**, *188*, 709–728. [CrossRef]
70. Kim, J.Y.; Lee, J.H.; Kim, J.H.; Mirzaei, A.; Kim, H.W.; Kim, S.S. Realization of H_2S sensing by Pd-functionalized networked CuO nanowires in self-heating mode. *Sens. Actuators B Chem.* **2019**, *299*, 126965. [CrossRef]
71. Romain, A.C.; Nicolas, J. Long term stability of metal oxide-based gas sensors for e-nose environmental applications: An overview. *Sens. Actuators B Chem.* **2010**, *146*, 502–506. [CrossRef]
72. Mirzaei, A.; Park, S.; Sun, G.-J.; Kheel, H.; Lee, C. CO gas sensing properties of $In_4Sn_3O_{12}$ and TeO_2 composite nanoparticle sensors. *J. Haz. Mater.* **2016**, *305*, 130–138. [CrossRef] [PubMed]
73. Mirzaei, A.; Kim, S.S.; Kim, H.W. Resistance-based H_2S gas sensors using metal oxide nanostructures: A review of recent advances. *J. Haz. Mater.* **2018**, *357*, 314–331. [CrossRef] [PubMed]
74. Mirzaei, A.; Janghorban, K.; Hashemi, B.; Bonyani, M.; Leonardi, S.G.; Neri, G. A novel gas sensor based on Ag/Fe_2O_3 core-shell nanocomposites. *Ceram. Int.* **2016**, *42*, 18974–18982. [CrossRef]
75. Mirzaei, A.; Kim, J.-H.; Kim, H.W.; Kim, S.S. How shell thickness can affect the gas sensing properties of nanostructured materials: Survey of literature. *Sens. Actuators B Chem.* **2018**, *258*, 270–294. [CrossRef]
76. Chen, D.; Yu, W.; Wei, L.; Ni, J.; Li, H.; Chen, Y.; Tian, Y.; Yan, S.; Mei, L.; Jiao, J. High sensitive room temperature NO_2 gas sensor based on the avalanche breakdown induced by Schottky junction in TiO_2-Sn_3O_4 nanoheterojunctions. *J. Alloys Compd.* **2022**, *912*, 165079. [CrossRef]

77. Choi, M.S.; Bang, J.H.; Mirzaei, A.; Oum, W.; Na, H.G.; Jin, C.; Kim, S.S.; Kim, H.W. Promotional effects of ZnO-branching and Au-functionalization on the surface of SnO_2 nanowires for NO_2 sensing. *J. Alloys Compd.* **2019**, *786*, 27–39. [CrossRef]
78. Xuan, J.; Zhao, G.; Sun, M.; Jia, F.; Wang, X.; Zhou, T.; Yin, G.; Liu, B. Low-temperature operating ZnO-based NO_2 sensors: A review. *RSC Adv.* **2020**, *10*, 39786–39807. [CrossRef]
79. An, S.; Park, S.; Ko, H.; Jin, C.; Lee, W.I.; Lee, C. Enhanced gas sensing properties of branched ZnO nanowires. *Thin Solid Films* **2013**, *547*, 241–245. [CrossRef]
80. Singh, N.S.; Kumar, L.; Kumar, A.; Vaisakh, S.; Singh, S.D.; Sisodiya, K.; Srivastava, S.; Kansal, M.; Rawat, S.; Singh, T.A. Fabrication of zinc oxide/polyaniline (ZnO/PANI) heterojunction and its characterisation at room temperature. *Mater. Sci. Semi. Proc.* **2017**, *60*, 29–33. [CrossRef]
81. Yang, M.; Zhang, X.; Guo, C.; Cheng, X.; Zhu, C.; Xu, Y.; Major, Z.; Huo, L. Resistive room temperature DMA gas sensor based on the forest-like unusual n-type PANI/TiO_2 nanocomposites. *Sens. Actuators B Chem.* **2021**, *342*, 130067. [CrossRef]
82. Zhang, W.; Cao, S.; Wu, Z.; Zhang, M.; Cao, Y.; Guo, J.; Zhong, F.; Duan, H.; Jia, D. High-performance gas sensor of polyaniline/carbon nanotube composites promoted by interface engineering. *Sensors* **2019**, *20*, 149. [CrossRef] [PubMed]
83. Fratoddi, I.; Venditti, I.; Cametti, C.; Russo, M.V. Chemiresistive polyaniline-based gas sensors: A mini review. *Sens. Actuators B Chem.* **2015**, *220*, 534–548. [CrossRef]
84. Saaedi, A.; Shabani, P.; Yousefi, R. High performance of methanol gas sensing of ZnO/PAni nanocomposites synthesized under different magnetic field. *J. Alloys Compd.* **2019**, *802*, 335–344. [CrossRef]
85. Cao, P.; Cai, Y.; Pawar, D.; Han, S.; Xu, W.; Fang, M.; Liu, X.; Zeng, Y.; Liu, W.; Lu, Y. Au@ ZnO/rGO nanocomposite-based ultra-low detection limit highly sensitive and selective NO_2 gas sensor. *J. Mater. Chem. C* **2022**, *10*, 4295–4305. [CrossRef]
86. Yang, X.; Salles, V.; Kaneti, Y.V.; Liu, M.; Maillard, M.; Journet, C.; Jiang, X.; Brioude, A. Fabrication of highly sensitive gas sensor based on Au functionalized WO_3 composite nanofibers by electrospinning. *Sens. Actuators B Chem.* **2015**, *220*, 1112–1119. [CrossRef]
87. Kim, J.-H.; Lee, J.-H.; Mirzaei, A.; Kim, H.W.; Kim, S.S. SnO_2 (n)-NiO (p) composite nanowebs: Gas sensing properties and sensing mechanisms. *Sens. Actuators B Chem.* **2018**, *258*, 204–214. [CrossRef]
88. Mirzaei, A.; Bang, J.H.; Choi, M.S.; Han, S.; Lee, H.Y.; Kim, S.S.; Kim, H.W. Changes in characteristics of Pt-functionalized RGO nanocomposites by electron beam irradiation for room temperature NO_2 sensing. *Ceram. Int.* **2020**, *46*, 21638–21646. [CrossRef]